International Journal of Thermal Sciences 49 (2010) 692–701

Contents lists available at ScienceDirect

International Journal of Thermal Sciences

journal homepage: www.elsevier.com/locate/ijts

Modelling of fin-and-tube evaporators considering non-uniform in-tube heat transfer

C. Oliet, C.D. Pérez-Segarra, J. Castro, A. Oliva*

Centre Tecnològic de Transferència de Calor (CTTC), Universitat Politècnica de Catalunya (UPC), ETSEIAT, Colom 11, 08222 Terrassa (Barcelona), Spain

ARTICLE INFO

Article history:
Received 28 May 2009
Received in revised form
9 November 2009
Accepted 15 November 2009
Available online 22 December 2009

Keywords:
Fin-and-tube heat exchangers
Evaporator
Numerical simulation
Flow pattern
Stratified flow

ABSTRACT

This paper is devoted to the presentation of a new model for fin-and-tube evaporators, focusing on the solid core simulation and its integration with a quasi-homogeneous two-phase flow model for the in-tube refrigerant flow. Special attention is given to separated in-tube flow patterns (stratified, stratified-wavy), because of their importance in liquid overfeed and domestic refrigerator evaporators and the impact on the solid core temperature distribution. The paper presents the solid core formulation and numerical method, the in-tube two-phase flow model, and describes the proposed integration algorithm between them. A selected single-tube baseline case is analysed in full detail, showing the impact of stratified flow on the fin-and-tube temperature distributions. Additional studies are finally presented analysing different flow transitions (single phase to stratified flow, stratified-wavy flow to annular flow, annular flow to partial dry-out) and several operating parameters (flow regime, tube material, tube thickness). Special attention is given to the influence of the flow pattern on the fin-and-tube core temperature profiles.

1. Introduction

This paper is devoted to the presentation of an advanced modelling and numerical strategy to simulate fin-and-tube evaporators (typically formed by a finned round tube bank), focusing on the analysis of the solid core, the refrigerant, and their integration, specially for separated flow situations (stratified, stratified-wavy flow patterns). This kind of flows is found in numerous equipment, i.e. industrial liquid overfeed evaporators [1] or domestic refrigerator evaporators [2]. In the first application, the use of ammonia as refrigerant is the dominant option.

Some recent works have been identified in the published literature on the calculation of plain transversal fins around tubes. Hoffenbecker et al. [3] presented a model for circular fin unsteady simulation including frost. The proposed discretisation was axisymmetric and assumed adiabatic fin edge for each tube zone. A bi-dimensional simulation was presented in Liang et al. [4] for steady state, centering the work on a comparison of the effects of several assumptions on the fin efficiency: 1D/2D model, air distribution properties, or rectangular/circular shape. Sommers and Jacobi [5] studied analytically a two-dimensional frost layer onto a one-dimensional circular fin, obtaining the corresponding fin efficiency.

In previous versions of the authors' model the fin was evaluated either by using fin efficiency concept, or by carrying out a 2D steady heat conduction simulation to detect possible transversal heat transfer bridges between tubes at different temperature (Oliet et al. [6]). A similar numerical procedure has also been recently published by Singh et al. [7]. Domanski et al. [8] analysed experimentally the longitudinal heat transfer effects in this kind of heat exchangers, reporting important impact in certain superheating conditions, as previously outlined analytically by Romero-Méndez et al. [9]. To the authors' knowledge, the current fin-tube model (see Oliet et al. [10] for a more detailed solid part analysis) is new in several aspects, e.g. fin cutting-cell discretisation, fin-tube coupling, and angular discretisation of the tubes.

Some papers have focused their attention on evaporation at low mass fluxes and low heat fluxes as being a characteristic range of fin-and-tube coils. Kelly et al. [1] carried out a work centered on the study of ammonia evaporation at air coil conditions, and their comparison against previous available correlations, which was found unsatisfactory. Ablanque et al. [11] have reported a critical examination of available experimental data on ammonia for this range (showing important divergences between datasets), and have carried out a revision of the performance of the available correlations, which also show considerable discrepancies. Bjork and Palm [2] have recently investigated the effect of turn bends on

* Corresponding author. Tel.: +34 937 398 192; fax: +34 937 398 101.
E-mail address: cttc@cttc.upc.edu (A. Oliva).
URL: http://www.cttc.upc.edu

1290-0729/$ – see front matter © 2009 Elsevier Masson SAS. All rights reserved.
doi:10.1016/j.ijthermalsci.2009.11.009

Nomenclature

A	area (m^2)
a,b,c	components of second order scheme (−)
c_p	heat capacity at constant pressure (J kg^{-1} K^{-1})
D	diameter (m)
d	distance (m)
e_c	specific kinetic energy (J kg^{-1})
e_p	specific potential energy (J kg^{-1})
F_p	fin pitch (m)
F_t	fin thickness (m)
f	friction factor (−)
G	mass velocity (kg m^{-2} s^{-1})
g	gravity (m s^{-2})
h	specific enthalpy (J kg^{-1})
L	length (m)
m	mass (kg)
$\dot{m}$	mass flow (kg s^{-1})
$\vec{n}$	surface unit vector (−)
p	pressure (N m^{-2})
$\dot{Q}$	heat rate (W)
R	thermal resistance (K/W)
r	radius (m)
S	section (m^2)
$\vec{s}$	direction unit vector (−)
T	temperature (K)
t	time (s)
V	volume (m^3)
v	velocity (m s^{-1})
x	vapour mass fraction (−)
z	axial position (m)

Greek

α	heat transfer coefficient (W m^{-2} K^{-1})
ϵ	void fraction (−)
λ	thermal conductivity (W m^{-1} K^{-1})
ρ	density (kg m^{-3})
θ	angle (rad)
τ	shear stress (N m^{-2})
ϕ	angle, generic magnitude (rad)

Subscripts

ANG	angular
AX	axial
a	air-side
b	fin-tube junction
F	fin, neighbour point
f	face
g	vapour phase
i	counter
l	liquid phase
n,s,e,w	neighbour faces
P	central point
r	refrigerant
w	wall

the stratified flow through a non-circular tube of a domestic refrigerator evaporator. Their experimental data revealed higher heat transfer coefficients comparing to previous correlations, which they assign to an additional perimeter wetted by liquid oscillations. Additional studies have centered on the use of microfin tubes in these flow conditions. Kelly et al. [1] tested experimentally the heat transfer enhancement by using microfin, specially at low mass fluxes. Honda and Wang [12] have presented an advanced theoretical model for the prediction of heat transfer in stratified flow within these kind of tubes. In the present paper, the flow-pattern map based correlation proposed by Thome [13] has been used due to the conclusions found in Ablanque et al. [11], and because it allows an accurate evaluation of the dry angle and the corresponding dry/wet heat transfer coefficients, which could be integrated with the angular tube discretisation approach.

This paper is devoted to the presentation of a novel model of fin-and-tube evaporators. The work is centered on the integration of the fin-tube solid core with an internal two-phase flow model, considering in-tube non-uniform heat transfer coefficients. The air-side has been simplified conveniently in each section. The model is presented in detail, focusing on the link between the fins and tubes, and between tubes and refrigerant. For a baseline ammonia evaporator, some verification studies have been carried out analysing the influence of grid density on results. For the same heat exchanger, the obtained results for a reference case are presented in detail. Finally, some flow transitions have been analysed, and the influence of some design conditions investigated.

2. Mathematical formulation and numerical procedure

In this section the mathematical model is presented, together with the proposed numerical methodology. The fin and tube models are described giving special attention to their coupling. The in-tube refrigerant flow model is also presented, emphasizing the link with the tubes, considering angular variation of the tube temperature and the internal heat transfer coefficients.

2.1. Solid elements

A more detailed formulation of this part can be found in another paper developed by the authors [10], which focuses on the solid part of the model, giving more detail of certain aspects of the formulation. It also includes additional verification studies and results on the code ability to predict fin efficiencies in continuous fins, and the transient behaviour of the solid core. In the current paper a presentation of this part is given for completeness and for clarifying the presentation of the coupling with the in-tube refrigerant flow model.

The mathematical formulation of this problem, as being the study of the solid elements in the fin-and-tube heat exchanger, is based on the general heat diffusion equation. The radiative heat transfer contribution has been neglected, and no internal heat sources are considered. Convective heat transfer interactions with the air or liquid flows are formulated through Newton's law of cooling.

2.1.1. Fin discretised equations

One way to reduce the amount of computational resources needed in the transient simulation of the fins is to reduce the number of grid nodes. The discretisation approach used previously by the authors was the so-called “blocking-off” method (in-out of the tube area) [6,14]. In order to assure an accurate result, a very fine mesh was required with the corresponding increase of computational time. The current approach moves to a “cutting-cell” method, i.e. generating new cells around the tubes which adapt to the tube shape (Fig. 1). With this discretisation, the fin base heat transfer can be stated in a clear and rigorous way by using the temperature gradient at that point.

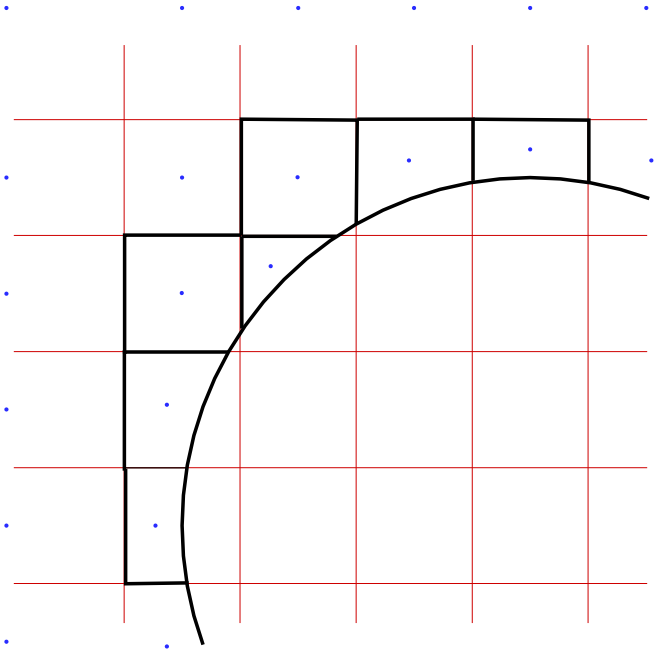

Fig. 1. New cutting-cell discretisation scheme.

The diffusive heat flux through fin cell faces, considering non-orthogonality, has been calculated by the following expression (incoming heat) ([15], scheme D3b).

$$\dot{Q}_f \approx \lambda_f \frac{(T_F - T_P)}{d_{PF}} \widehat{A}_f + \lambda_f \overline{\nabla T}_f \cdot \left[A_f \vec{n}_f - \widehat{A}_f \vec{s}_f \right] \tag{1}$$

where $\dot{Q}_f$ represents the heat flux through cell face 'f' between the main node 'P' and its neighbour 'F'. The area $\widehat{A}_f$ is defined as $\widehat{A}_f = A_f/(\vec{n}_f \cdot \vec{s}_f)$. The unit vector $\vec{n}_f$ is normal to the cell face, while $\vec{s}_f$ is a unit vector from node P to node F. The interpolated gradient at cell face is calculated from the gradients at cell centroids (following the interpolation criterion I1 indicated in [15]). The temperature gradients at cell centroids are obtained by the least squares technique from neighbour fin nodes (centroids or fin bases), considering the corresponding temperatures and distances.

Applying the heat diffusion equation to a general fin cell (Fig. 2), the corresponding discretised equation is obtained:

$$\rho_P c_{p,P} \frac{aT_P - bT_P^0 + cT_P^{00}}{\Delta t} V_P = (\dot{Q}_s + \dot{Q}_n + \dot{Q}_w + \dot{Q}_e) + \sum \dot{Q}_{bF,i} - \dot{Q}_a \tag{2}$$

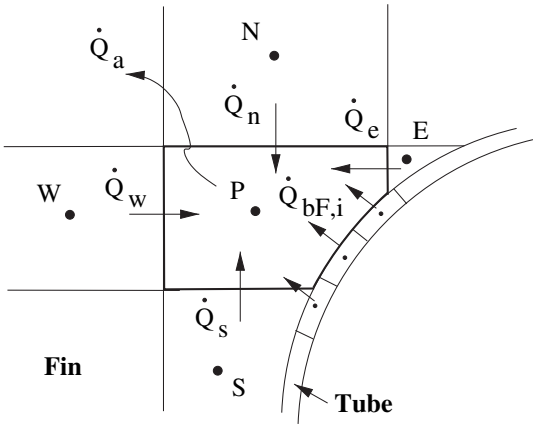

Fig. 2. Fin control volume with main heat transfer interactions.

where the conduction terms at cell faces are evaluated using Eq. (1) and coefficients a, b, and c stand for first order ($a = 1, b = 1, c = 0$), or second order ($a = 1.5, b = 2, c = 0.5$) accuracy for the unsteady term. The $\dot{Q}_{bF,i}$ term stands for the heat transfer through the fin base coming from different tube cells, and $\dot{Q}_a$ for the air-side convective heat transfer.

2.1.2. Tube discretised equations

Each tube within the finned tube bank has been solved numerically with a 2D (axial + angular directions) discretisation (Fig. 3). The thin fin hypothesis has been considered in radial direction (uniform temperature).

The heat diffusion equation has again been applied to each control volume, considering the heat conduction interaction with tube neighbour nodes, the heat conduction to fin cells base ($\dot{Q}_b$), and the convective heat transfer from/to the air and refrigerant flows ($\dot{Q}_a$ and $\dot{Q}_r$). The discretised equation is presented in Eq. (3), where the temperature derivative with time has also been approximated by a second order scheme.

$$\rho_P c_{p,P} \frac{aT_P - bT_P^0 + cT_P^{00}}{\Delta t} V_P = (\dot{Q}_s + \dot{Q}_n + \dot{Q}_w + \dot{Q}_e) + \dot{Q}_r - \dot{Q}_a - \dot{Q}_b \tag{3}$$

2.1.3. Tube-fin junction

The heat transfer to the fin cells base (fin-tube junction) can be expressed in terms of the thermal contact resistance to the fin cell base temperature T_b. This heat quantity is at the same time transferred from fin base to surrounding air and to the fin core, obtaining an additional equation Eq. (4). The relation to the fin core is presented in terms of temperature gradient at fin base, obtained by least squares technique from neighbour fin nodes (centroids or fin bases). With this approach, the evaluation of the heat transfer to the fins is more accurate and better linked with fin temperature field.

$$\dot{Q}_b = \dot{Q}_{bF} + \dot{Q}_{ba} = -\lambda(\nabla T|_b \cdot \vec{r}) A_{bF} + \alpha_a (T_b - T_a) A_{ba} \tag{4}$$

2.2. Two-phase flow

A quasi-homogeneous two-phase flow model has been implemented [16] for the resolution of the thermal and fluid dynamic behaviour of two-phase flow inside ducts. The main flow values are obtained from the integration of the fluid conservation equations (momentum, continuity and energy) along the tube domain over a finite control volume, as shown in Fig. 4.

Considering that the transient term is evaluated from the previous time step ($\partial\phi/\partial t \approx (\phi - \phi^0)/\Delta t$), and that the control volume values are obtained from an arithmetic mean between the inlet $i-1$ and outlet i faces ($\overline{\phi} \approx (\phi_i + \phi_{i-1})/2$), the semi-discretised governing equations show the following form:

$$\frac{\partial \overline{m}}{\partial t} + \dot{m}_i - \dot{m}_{i-1} = 0 \tag{5}$$

$$\frac{\partial \overline{m}\overline{v}}{\partial t} + \dot{m}_{g,i} v_{g,i} + \dot{m}_{l,i} v_{l,i} - \dot{m}_{g,i-1} v_{g,i-1} - \dot{m}_{l,i-1} v_{l,i-1} = (p_{i-1} - p_i) S - \overline{\tau} \pi D \Delta z - mg \sin\theta \tag{6}$$

$$\frac{\partial \overline{m}(\overline{h} + \overline{e}_c + \overline{e}_p)}{\partial t} + \dot{m}_i (h + e_c + e_p)_i - \dot{m}_{i-1} (h + e_c + e_p)_{i-1} = -\dot{Q}_r + V \frac{\partial p}{\partial t} \tag{7}$$

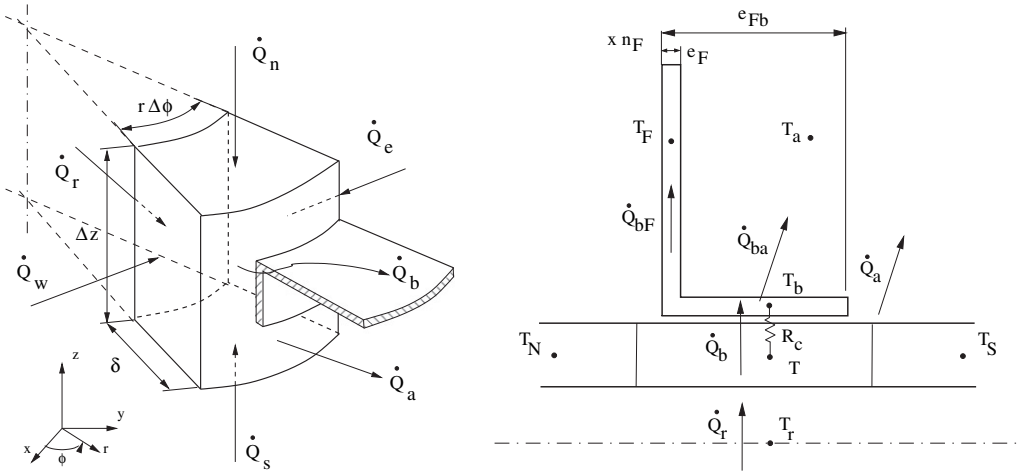

Fig. 3. Tube control volume with main heat transfer interactions.

The mean flow velocity of each phase is expressed by means of both the mass weight fraction and the void fraction e.g. $v_{l,i} = (\dot{m}_i(1 - x_{g,i}))/(\rho_l(1 - \epsilon_{g,i})S)$. This formulation requires the use of empirical correlations to evaluate three specific parameters: the void fraction (ϵ), the shear stress (usually calculated from a friction factor $\bar{\tau} = (f/4)(\dot{m}^2/2\rho S^2)$), and the convective heat transfer coefficient used to evaluate the heat transfer between the tube and the fluid.

The flow is evaluated on the basis of a step-by-step numerical implicit scheme. The resulting governing equations are rearranged and solved for the i position. Thus, from the duct flow inlet conditions, namely pressure, enthalpy and mass flow, each control volume outlet state is calculated sequentially. The tube wall temperature map acts as the boundary condition for the whole internal flow at each iteration.

2.2.1. Non-uniform in-tube heat transfer coefficients

During in-tube saturated boiling conditions, the inner perimeter can be fully or partially wetted depending on the flow pattern type. Because of the low mass flow velocities frequently encountered in fin-and-tube evaporators, stratified or stratified-wavy flow are usually found, which are paradigmatic cases of separated vapour/liquid flow.

Flow pattern map based correlations, i.e. those presented by Thome [13], evaluate both contributions: the heat transfer occurring through the portion of the tube inner perimeter in contact with the liquid phase (α_l), and the vapour heat transfer coefficient through the dry part of the perimeter (α_g). The average heat transfer coefficient is calculated proportionally to the dry angle (θ_{dry}), which is obtained from the corresponding flow pattern map and flow conditions. In that particular correlation, the value of α_g is directly calculated with the Dittus and Boelter correlation [17], while α_l is determined by means of the asymptotic model proposed by Steiner and Taborek [18].

In this work, instead of using the average heat transfer coefficient, each tube control volume takes the corresponding dry or wet heat transfer coefficient depending on their angular position. Moreover, if a tube control volume is partially dry/wet, an average heat transfer coefficient is derived from dry/wet area ratio.

As expected, the in-tube fluid also considers the local tube temperatures when calculating the heat transfer values. For most cases, where the heat transfer coefficients of one zone are considered uniform, the expression of heat gains/losses through the wall can be expressed in a condensed way by means of average dry and wet wall temperatures. This allows an easier implementation into the refrigerant module.

$$\dot{Q}_r = \dot{Q}_{r,g} + \dot{Q}_{r,l} = \sum_g \alpha_g (T - T_{w,i}) A_i + \sum_l \alpha_l (T - T_{w,i}) A_i = \alpha_g (T - \overline{T}_{w,g}) A_g + \alpha_l (T - \overline{T}_{w,l}) A_l \quad (8)$$

2.3. Global algorithm-convective interactions

The coupling of the air and refrigerant with the solid elements has been carried out by using a segregated algorithm. However, the tube and fins can be solved in a segregated or in a coupled way. At current stage, both fluid flows have been discretised by using

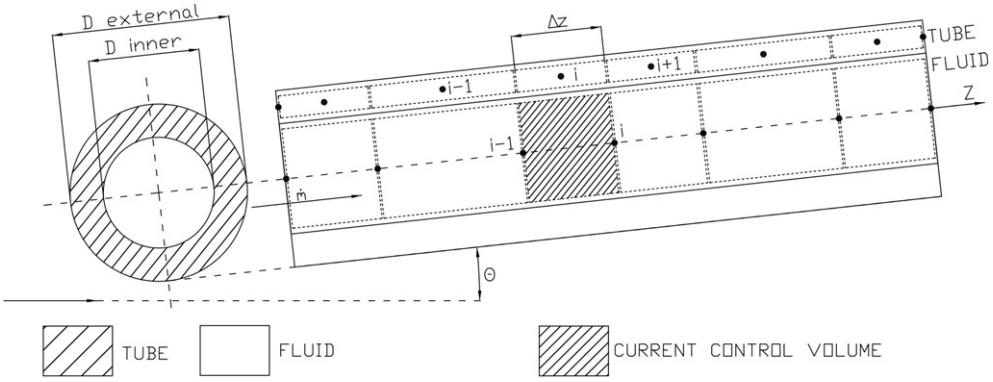

Fig. 4. Refrigerant flow discretisation.

Table 1
Baseline case geometry and working conditions.

D_o	22.0 mm
D_i	19.4 mm
F_p	8.0 mm
F_t	0.35 mm
L_x	65.0 mm
L_y	65.0 mm
L_z	10.0 m
α_a	70.0 W m^{-2} K^{-1}
T_a	0.0 °C
$T_{r,i}$	−10.0 °C
$h_{r,i}$	154 010 J kg^{-1}, sat. liquid (IIR ref.)
$\dot{m}_r$	4.5e-3 kg s^{-1}
fluid	R717
fin-tube	steel

a one-dimensional approach. Applying the corresponding mass, energy and conservation equations, the velocity, pressure and temperature fields are obtained. The convective interactions of the solid elements with the surrounding air and refrigerant flows have been stated by using Newton's law of cooling. The necessary empirical information has been obtained from selected correlations. The current paper is centered on the analysis of the coupling of the solid core with the in-tube refrigerant, being the airflow conveniently simplified to obtain representative results.

3. Results

A single-tube heat exchanger representative of an ammonia liquid overfeed evaporator has been selected in order to show the capabilities of the model in determining the fin, tube and in-tube refrigerant local conditions. Table 1 indicates the geometry and working conditions for the baseline case. Regarding previous comment on the airflow simplification, the results presented herewith have considered constant and uniform air-side conditions.

3.1. Verification

Before presenting the selected results, the quality of the obtained numerical solutions has to be addressed by using a verification procedure. In this case, a triple mesh analysis has been carried out on the baseline case, changing the number of grid nodes in tube axial and angular directions, and varying the number of grid nodes in the fins (fractions of diameter). In these verification cases, the length of the test has been reduced to 1 m in order to allow sufficient axial densification.

The results (Fig. 5) indicate an adequate convergence towards asymptotic results for the three meshes under analysis, and notable accuracy even for low number of grid nodes. As expected from previous studies on the fin-and-tube solid core, the fin grid has the highest impact on the end results, asking for $N_F \geq 20$ (mesh size in diameter fractions) to obtain the desired result with the highest level of accuracy, or $N_F \geq 10$ to obtain a reasonably accurate result with less computational requirements. For the angular discretisation, the results show good stability even for the lowest values. However, to obtain the grid independent result $N_{ANG} \geq 40$ is recommended. In this case, the axial discretisation shows a high stability, requiring $N_{AX} \geq 40$ control volumes to obtain grid independent value. It has been detected, for cases with sudden changes in heat transfer coefficients (e.g. single phase to two-phase flow), that the axial discretisation should be denser in order to fix adequately such abrupt transitions.

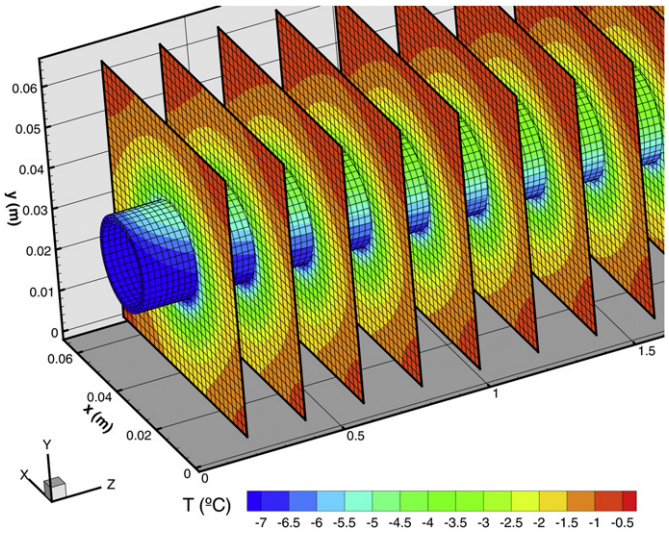

Fig. 6. Detail of the fin-and-tube HEX analysis. Discretisation of tubes and fins and temperature maps.

3.2. Baseline case analysis

The baseline case is analysed in this section with full detail, in order to show the model approach and level of analysis, as well as to present some aspects related to the in-tube flow non-uniformity. Regarding the discretisation approach and the coupling between tubes and fins, a small portion of the heat exchanger is depicted in Fig. 6, which includes the used meshes and the obtained temperature maps. Only several fins have been included for the sake of clarity. The obtained level of detail allows for integration of in-tube

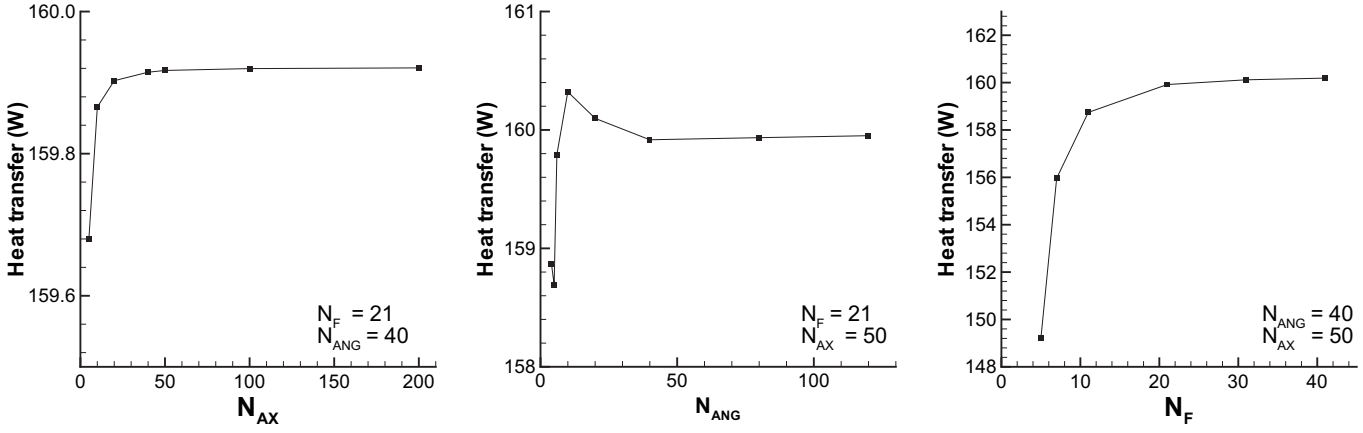

Fig. 5. Verification of solutions:from left to right, axial (N_{AX}), angular (N_{ANG}), and fin (N_F) grid density influence.

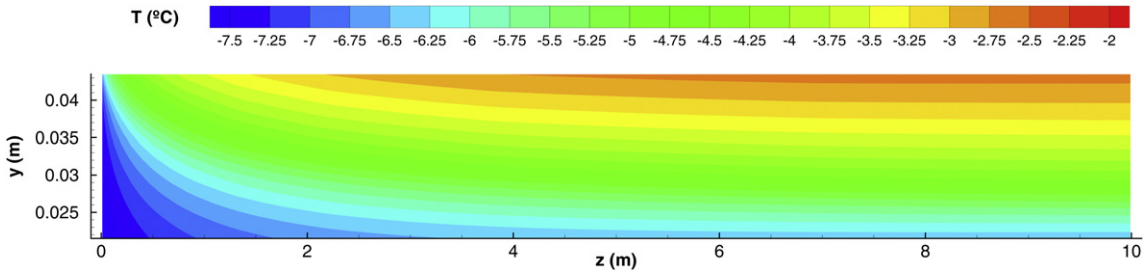

Fig. 7. Tube temperature map for the baseline case, lateral projection.

separated flow and avoids the introduction of analytical fin efficiencies.

The tube temperature map along the exchanger is given in Fig. 7 (lateral projection), where the influence of the stratified flow in the temperature pattern is clearly observed. The in-tube top gas flow, with lower heat transfer coefficients, increases the refrigerant relative thermal resistance thus displacing the temperatures at the top towards the air side. The dry surface (and consequently the dry angle) spreads with tube length as the internal vapour mass fraction increases.

The fin temperature maps at certain axial positions are provided in Fig. 8. They also show the effects of the in-tube heat transfer non-uniformity. From an inlet almost uniform and symmetric map, the separation of in-tube flow produces at longer distances a clear top-bottom asymmetry in the fin temperature maps. This aspect is considered of importance in the end performance of the heat exchanger, as well as in the frost formation distribution.

The refrigerant conditions along the tube are also shown in Fig. 9. The enthalpy and vapour mass fraction increase as a result of the evaporation process, while the dry angle expansion indicates the evolution of the stratified flow inside the tube. The internal heat transfer non-uniformity is clearly observed both in the progressive separation of the wall mean dry/wet temperatures, and in the reduction of the average heat transfer coefficient.

In order to close the presentation of the baseline case, the previous results considering the in-tube heat transfer coefficients non-uniformity are compared to the uniform heat transfer coefficient approach (Fig. 10). In the latter case, the average refrigerant heat transfer coefficient is fixed for all angular positions. The results show the highest impact of the non-uniform approach on the wall temperatures, being lower on the dry angle evolution and on the in-tube heat transfer coefficients.

3.3. Flow pattern transitions

The interest at this point is the study of flow transitions with abrupt changes in the dry angle, where the proposed model offers singular analysis capabilities. Three different transitions have been investigated: i) from subcooled liquid to stratified flow (SC-S); ii) from stratified-wavy flow to annular flow (SW-A); iii) from annular flow to partial dry-out (A-DO). For each case, the inlet flow conditions have been selected with the background of the corresponding flow pattern map [13].

For the first transition the conditions are the same as the baseline case, with the exception of entering as a subcooled liquid at −14 °C. Fig. 11 analyses this case near the transition. The evolution of refrigerant temperature clearly reflects the heating during single phase flow, while as expected the temperature

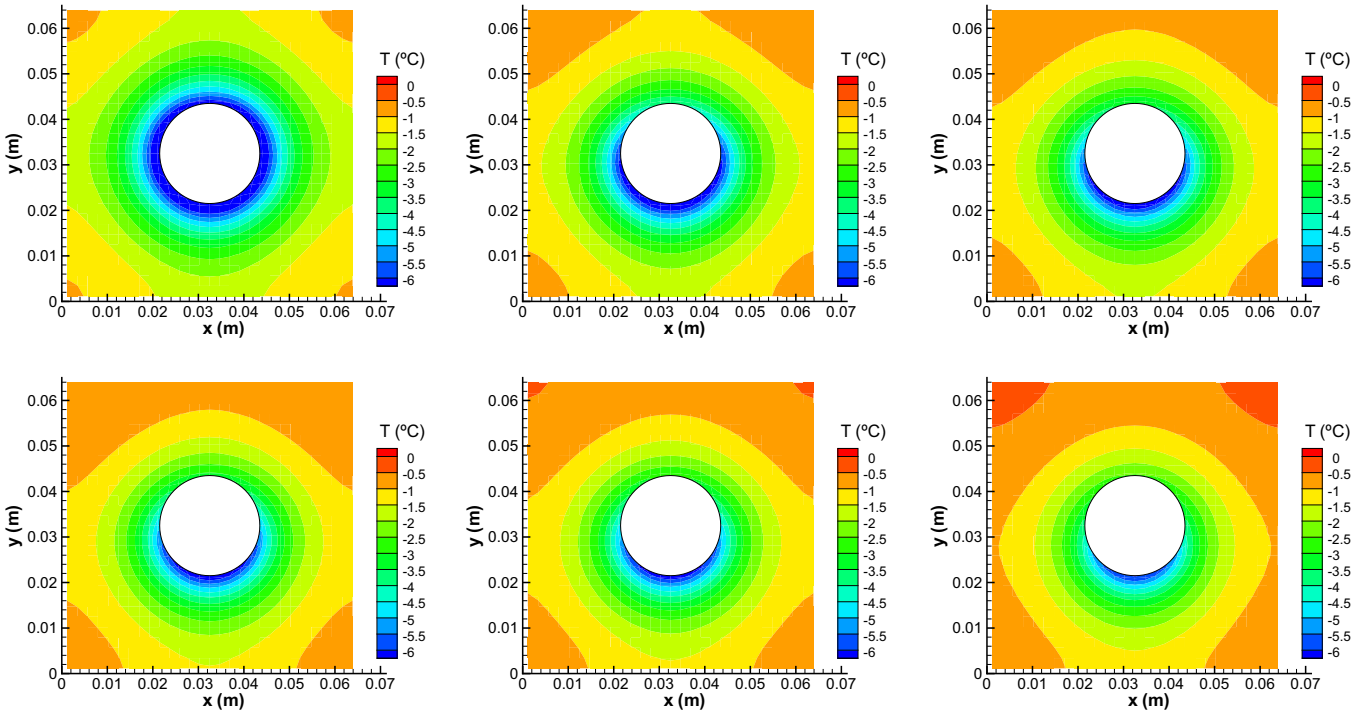

Fig. 8. Fin temperature maps for the baseline case at different axial locations (from left to right and from top to bottom:0/0.5/1/1.5/2 and 10 m).

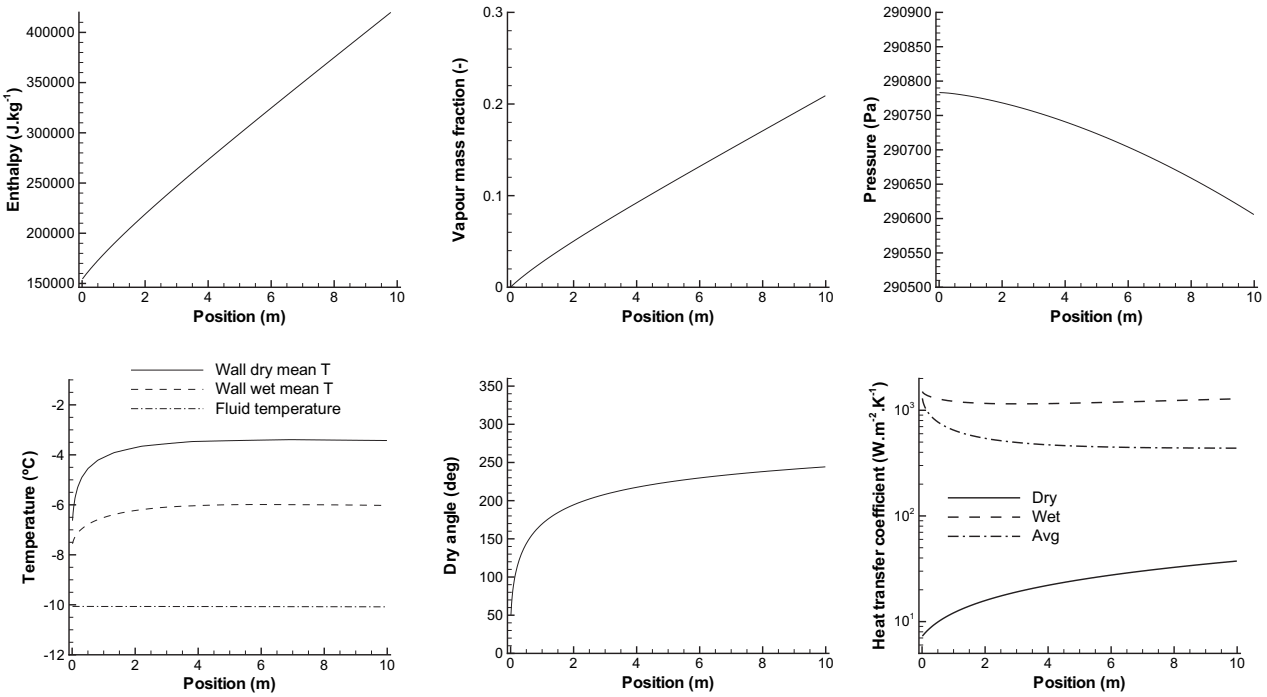

Fig. 9. Local variation of in-tube refrigerant conditions.

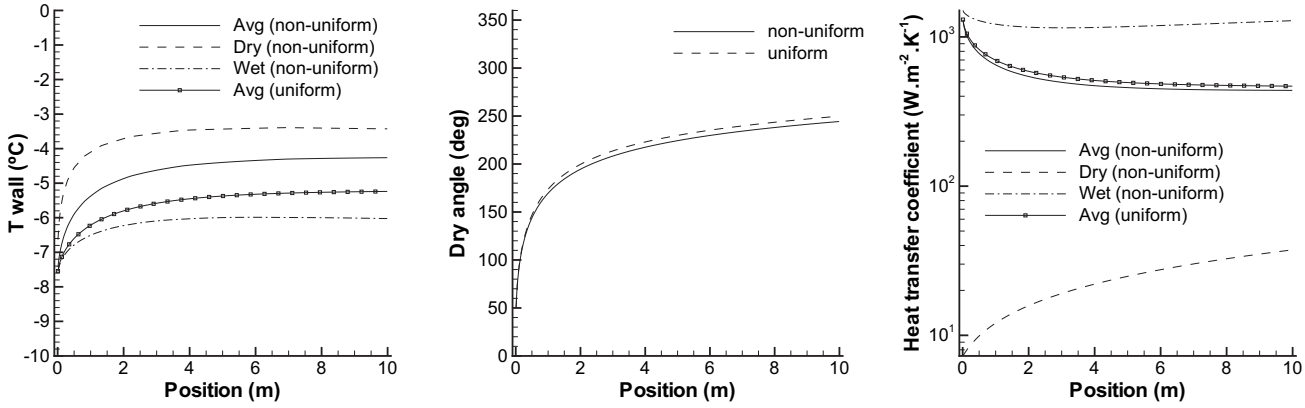

Fig. 10. Comparison of non-uniform vs. uniform in-tube heat transfer coefficient approach.

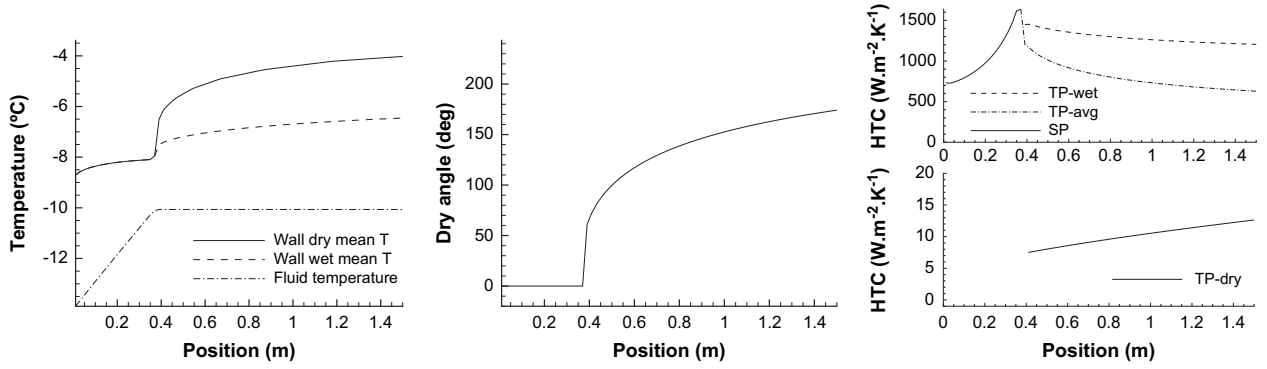

Fig. 11. Transition from subcooled liquid to two-phase stratified region (SC-S).

remains almost constant for the short two-phase flow length depicted. Having a stratified flow, the mean wall dry and wet temperatures separate within the two-phase region, while the dry angle increases with length. The heat transfer coefficient also reveals a strong dependency of the flow pattern/phenomenon. The influence of the dry area reduces progressively the average heat transfer coefficient in the two-phase region. In the single phase zone, subcooled boiling is reflected in the increasing heat transfer coefficients towards the two-phase region.

The second transition is evaluated at the baseline conditions, but with $G = 90\,\mathrm{kg\,m^{-2}\,s^{-1}}$ and inlet vapour mass fraction of 0.35. At these conditions, the transition from stratified-wavy to annular flow can be evaluated. As seen in Fig. 12, the dry angle decreases to zero where the annular flow starts. Up to this point, the influence of the dry angle is reflected by the separation from wall mean dry/wet temperatures, and again in the decrease of the average heat transfer coefficient.

The last transition of interest considers the change from annular flow to partial dry-out (horizontal tube). The conditions are again taken from the baseline case, but fixing $G = 90\,\mathrm{kg\,m^{-2}\,s^{-1}}$ and inlet vapour mass fraction of 0.9. Fig. 13 depicts the strong influence of the dry-out onset. Within the annular flow ($\theta_{dry} = 0$), the high heat transfer coefficients are reflected by a small temperature difference between the wall and the refrigerant. Conversely, as the partial dry-out starts, the dry angle rapidly increases producing a sudden drop of the average heat transfer coefficients which also creates, as expected, a sudden increase of the dry wall temperature.

3.4. Design alternatives

In this section, the impact of several design parameters on the refrigerant and solid thermal behaviour has been investigated. The first study has been centered on the variation of the refrigerant

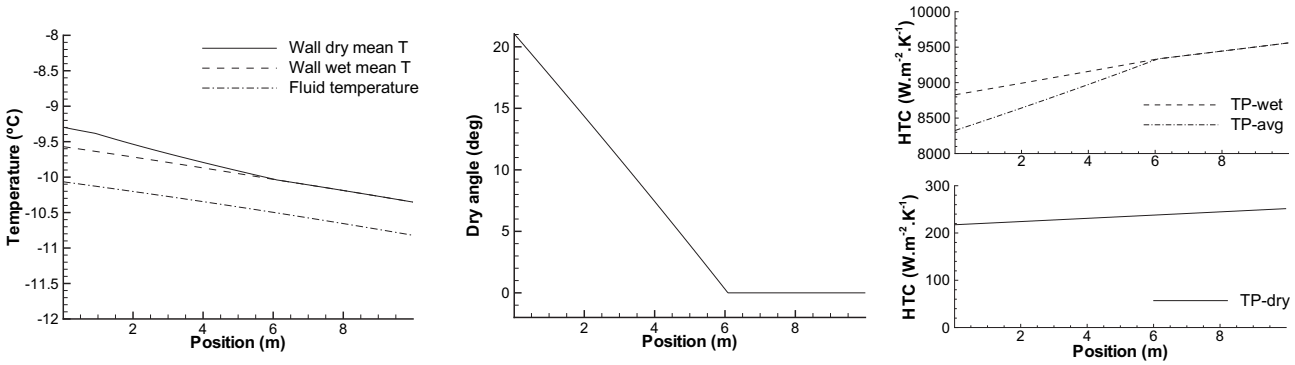

Fig. 12. Transition from stratified-wavy to annular flow (SW-A).

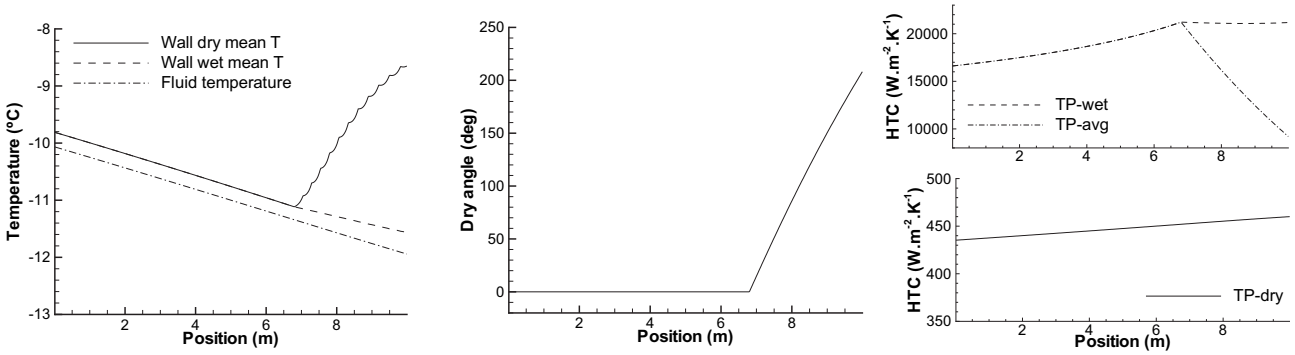

Fig. 13. Transition from annular flow to dry-out region (A-DO).

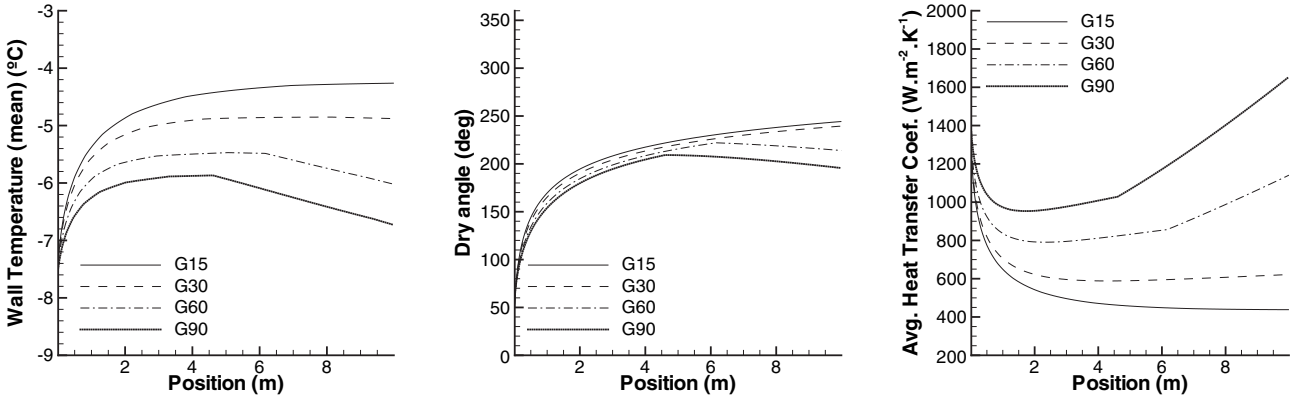

Fig. 14. Influence of refrigerant mass flow.

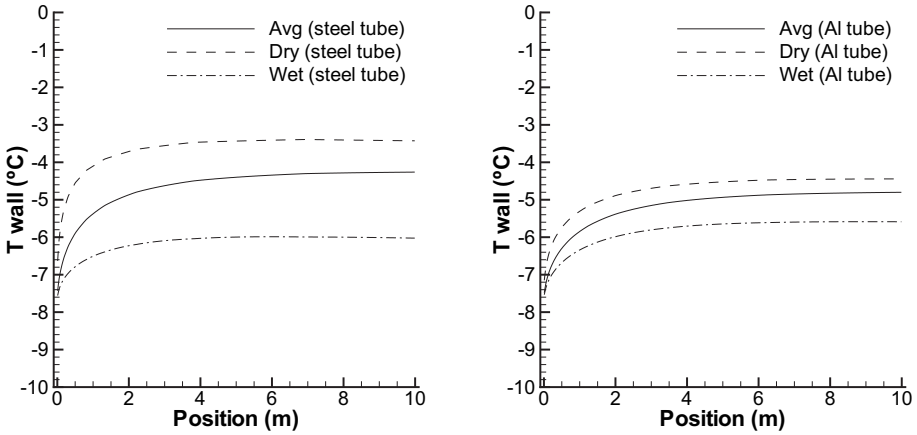

Fig. 15. Influence of tube material: steel tube (left) vs. aluminium tube (right).

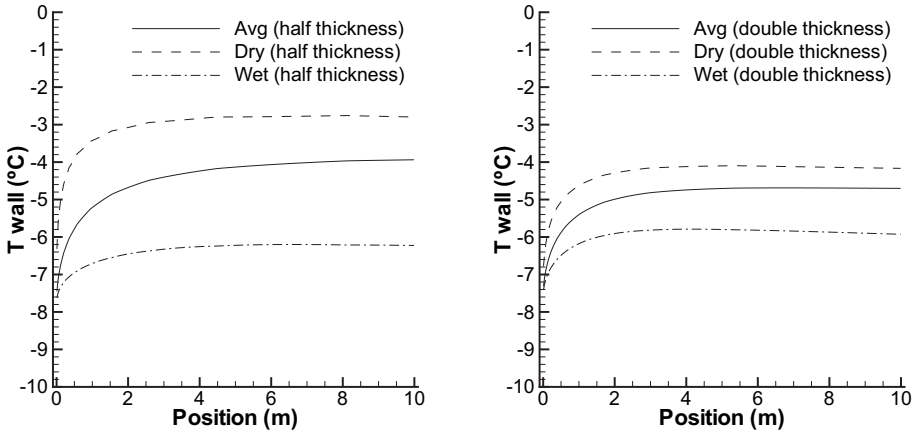

Fig. 16. Influence of tube thickness: half (left) vs. double (right) thickness.

mass flow, from $G = 15$ kg m^{-2} s^{-1} to 90 kg m^{-2} s^{-1}. In this particular case, the four flows under investigation start their flow path as stratified flow, increasing the dry angle with length, which causes a decrease in the average heat transfer coefficients and the corresponding increase in the mean tube temperature (Fig. 14). As expected, the higher the mass velocity, the higher the heat transfer coefficient, which produces a colder wall mean temperature because of the drop in refrigerant relative thermal resistance. For the $G = 60$ kg m^{-2} s^{-1} and $G = 90$ kg m^{-2} s^{-1} cases, the transition from stratified to stratified-wavy flow is identified in the change of trend of the dry angle, and the corresponding impact on the other variables.

Another aspect of interest is to analyse the impact of varying the tube thermal resistance, changing the tube material or the tube thickness. As seen in Figs. 15 and 16, the reduction (by increasing the thermal conductivity or the angular section) of the tube circumferential/angular thermal resistance (relation between temperature gradient and heat transfer in angular direction, in this case pure conductive resistance $R_\phi = r\Delta\phi/\lambda A$), creates a more homogeneous tube temperature (range between mean dry and wet wall temperatures) and a lower mean tube temperature level.

4. Conclusions

This paper presents in detail a new formulation in order to model in unsteady and very detailed way fin-and-tube evaporators. The work is focused on the link between the developed fin-and-tube solid core simulation with an in-tube quasi-homogeneous two-phase flow model, considering the possibility of separated liquid-vapour heat transfer coefficients. This is specially interesting in the stratified or stratified-wavy flows, very common patterns in liquid overfeed evaporators, and also found in domestic refrigerator evaporators.

The results are illustrative of the importance of considering the angular heat transfer coefficient non-uniformity. A baseline case corresponding to an ammonia liquid overfeed evaporator has been presented in full detail. Some transition flows have also been analysed to show the effects of abrupt changes in the in-tube heat transfer coefficients distribution. Finally, the influence of flow regime and relative refrigerant thermal resistance has been reported.

Acknowledgements

This research work has been partially funded by the Ministerio de Educación y Ciencia, Secretaría de Estado de Universidades e Investigación, Spain (refs. ENE2006-11099, ENE2005-08302).

References

[1] J.E. Kelly, S.J. Eckels, D.F. Fenton, An experimental investigation of in-tube evaporation of pure ammonia in a smooth and a microfin tube, part I - heat transfer (RP-866). International Journal of Heat Ventilation Air Conditioning and Refrigeration Research 8 (3) (2002) 239–256.

[2] E. Bjork, B. Palm, Flow boiling heat transfer at low flux conditions in a domestic refrigerator evaporator. International Journal of Refrigeration 31 (6) (2008) 1021–1032.
[3] N. Hoffenbecker, S.A. Klein, D.T. Reindl, Hot gas defrost model development and validation. International Journal of Refrigeration 28 (54) (2005) 605–615.
[4] S.Y. Liang, T.N. Wong, G.K. Nathan, Comparison of one-dimensional and two-dimensional models for wet-surface fin efficiency of a plate-fin-tube heat exchanger. Applied Thermal Engineering 20 (10) (2000) 941–962.
[5] A.D. Sommers, A.M. Jacobi, An exact solution to steady heat conduction in a two-dimensional annulus on a one-dimensional fin: application to frosted heat exchangers with round tubes. International Journal of Refrigeration 128 (4) (2006) 397–404.
[6] C. Oliet, C.D. Pérez-Segarra, S. Danov, A. Oliva, Numerical simulation of dehumidifying fin-and-tube heat exchangers. Model strategies and experimental comparisons, in: Proceedings of the 2002 International Refrigeration Engineering Conference at Purdue, 2002, CD-ROM, Ref. R5-5, pp. 1–8.
[7] V. Singh, V. Aute, R. Radermacher, Numerical approach for modeling air-to-refrigerant fin-and-tube heat exchanger with tube-to-tube heat transfer. International Journal of Refrigeration 31 (8) (2008) 1414–1425.
[8] P.A. Domanski, J.M. Choi, W.V. Payne, Longitudinal heat conduction in finned-tube evaporators, in: Proceedings of the 22nd International Congress of Refrigeration, 2007, pp. 1–8.
[9] R. Romero-Méndez, M. Sen, K.T. Yang, R.L. McClain, Effect of tube-to-tube conduction on plate-fin and tube heat exchanger performance. International Journal of Heat and Mass Transfer 40 (16) (1997) 3909–3916.
[10] C. Oliet, C.D. Pérez-Segarra, A. Oliva, J. Castro, Multidimensional and unsteady simulation of fin-and-tube heat exchangers. Numerical Heat Transfer, Part A 56 (3) (2009) 193–210.
[11] N. Ablanque, J. Rigola, C. Oliet, J. Castro, Critical analysis of available ammonia horizontal in-tube boiling heat transfer correlations for liquid overfeed evaporators. Journal of Heat Transfer – Transactions of ASME 130 (3) (2008) 345021–345025.
[12] H. Honda, Y.S. Wang, Theoretical study of evaporation heat transfer in horizontal microfin tubes: stratified flow model. International Journal of Heat and Mass Transfer 47 (17–18) (2004) 3971–3983.
[13] J. Thome, Update on advances in flow pattern based two-phase heat transfer models. Experimental Thermal and Fluid Science 29 (3) (2005) 341–349.
[14] C. Oliet, Numerical Simulation and Experimental Validation of Fin-and-Tube Heat Exchangers. Ph.D. thesis, Universitat Politècnica de Catalunya, (2006).
[15] C.D. Pérez-Segarra, C. Farré, J. Cadafalch, A. Oliva, Analysis of different numerical schemes for the resolution of convection - diffusion equations using finite volume methods on three dimensional unstructured grids. Part I: discretization schemes. Numerical Heat Transfer, Part B 49 (4) (2006) 333–350.
[16] O. García-Valladares, C.D. Pérez-Segarra, J. Rigola, Numerical simulation of double-pipe condensers and evaporators. International Journal of Refrigeration 27 (6) (2004) 656–670.
[17] P.W. Dittus, L.M.K. Boelter, Heat transfer in automobile radiators of the tubular type. International Communications in Heat and Mass Transfer 12 (1) (1985) 3–22.
[18] D. Steiner, J. Taborek, Flow boiling heat transfer in vertical tubes correlated by an asymptotic model. Heat Transfer Engineering 13 (2) (1992) 43–69.